Oligodendroglial connexin 47 regulates neuroinflammation upon autoimmune demyelination in a novel mouse model of multiple sclerosis

Yinan Zhao[a], Ryo Yamasaki[a], Hiroo Yamaguchi[a], Satoshi Nagata[a], Hayato Une[a], Yiwen Cui[a], Katsuhisa Masaki[a], Yuko Nakamuta[a], Kyoko Iinuma[a], Mitsuru Watanabe[a], Takuya Matsushita[a], Noriko Isobe[a], and Jun-ichi Kira[a,1]

[a]Department of Neurology, Neurological Institute, Graduate School of Medical Sciences, Kyushu University, 812-8582 Fukuoka, Japan

Edited by Lawrence Steinman, Stanford University School of Medicine, Stanford, CA, and approved December 20, 2019 (received for review February 7, 2019)

In multiple sclerosis plaques, oligodendroglial connexin (Cx) 47 constituting main gap junction channels with astroglial Cx43 is persistently lost. As mice with Cx47 single knockout exhibit no demyelination, the roles of Cx47 remain undefined. We aimed to clarify the effects of oligodendroglia-specific Cx47 inducible conditional knockout (icKO) on experimental autoimmune encephalomyelitis (EAE) induced by myelin oligodendrocyte glycoprotein peptide (MOG35-55) in PLP/CreERT;Cx47fl/fl mice at 14 d after tamoxifen injection. Cx47 icKO mice demonstrated exacerbation of acute and chronic relapsing EAE with more pronounced demyelination than Cx47 flox (fl)/fl littermates. CD3+ T cells more abundantly infiltrated the spinal cord in Cx47 icKO than in Cx47 fl/fl mice throughout the acute to chronic phases. CXCR3-CCR6+CD4+ and IL17+IFNγ-CD4+ helper T (Th) 17 cells isolated from spinal cord and brain tissues were significantly increased in Cx47 icKO mice compared with Cx47 fl/fl mice, while MOG35-55-specific proliferation and proinflammatory cytokine production of splenocytes were unaltered. Microarray analysis of isolated microglia revealed stronger microglial activation toward proinflammatory and injury-response phenotypes with increased expressions of chemokines that can attract Th17 cells, including Ccl2, Ccl3, Ccl4, Ccl7, and Ccl8, in Cx47 icKO mice compared with Cx47 fl/fl mice. In Cx47 icKO mice, NOS2+ and MHC class II+ microglia were more enriched immunohistochemically, and A1-specific astroglial gene expressions and astroglia immunostained for C3, a representative A1 astrocyte marker, were significantly increased at the acute phase, compared with Cx47 fl/fl mice. These findings suggest that oligodendroglia-specific Cx47 ablation induces severe inflammation upon autoimmune demyelination, underscoring a critical role for Cx47 in regulating neuroinflammation.

experimental autoimmune encephalomyelitis | connexin 47 | multiple sclerosis | microglia | astroglia

Multiple sclerosis (MS) is an autoimmune demyelinating disease affecting the central nervous system (CNS). We and others reported widespread alterations in glial connexins (Cxs) in demyelinating diseases such as MS, Baló concentric sclerosis, and neuromyelitis optica (1–3). Cxs are transmembrane molecules that form gap junction (GJ) channels to allow intercellular exchange of ions, secondary messengers, and energy sources (4). Acute MS plaques show more extensive loss of oligodendroglial Cx32 and Cx47 and astroglial Cx43 than demyelinated areas, although oligodendroglia and astroglia are still present (2, 3). Meanwhile, chronic MS lesions exhibit marked up-regulation of astroglial Cx43, reflecting progressive astrogliosis, and persistent loss of oligodendroglial Cx32 and Cx47 even in partially remyelinated shadow plaques (2, 3). Given that energy sources, such as glucose and lactate, are transferred from blood vessels to oligodendroglia and neurons via astroglia through Cx GJs, loss of oligodendroglia–astrocyte GJs may cause energy failure, resulting in myelin and axon loss (1, 3). However, the precise roles of glial Cx alterations in MS remain to be established.

Acute experimental autoimmune encephalomyelitis (EAE) was reported to be unaltered in astrocytic *Cx30* or *Cx43* single-knockout (KO) mice and even in *Cx30*/*Cx43* double-KO mice (5). We recently found that *Cx30* ablation attenuated the chronic, but not acute, phase of EAE through induction of neuroprotective microglia (6). By contrast, oligodendrocytic *Cx32* KO mice developed aggravated EAE with increased demyelination compared with wild-type (WT) mice, despite showing a degree of neuroinflammation similar to WT mice upon EAE induction and little clinical progression at the chronic phase (7). Markoullis et al. (7) assumed that remyelination failure may be responsible for the aggravation of EAE in oligodendroglial *Cx32* KO mice (7), although single KO of *Cx32* caused neither neurological abnormalities nor pathological changes (8).

Compared with Cx32, Cx47 showed more-abundant expression on the surface of oligodendroglial perikarya and proximal portions of processes and similar expression on the surface of myelin

Significance

In multiple sclerosis plaques, oligodendroglial connexin (Cx) 47 constituting main gap junction channels with astroglia is persistently lost. The roles of Cx47 remain undefined. Here, we show that oligodendroglia-specific conditional ablation of *Cx47* exacerbated acute and chronic relapsing experimental autoimmune encephalomyelitis induced by myelin oligodendrocyte glycoprotein peptide (MOG_{35-55}) immunization, with florid infiltration of $CD3^+$ T cells, especially helper T (Th) 17 cells, and pronounced demyelination without influencing MOG-specific T cell induction. Microarray and immunohistochemistry analyses revealed stronger activation of proinflammatory and injury-response microglia with increased expressions of chemokines that can attract Th17 cells, and A1 astroglia at the acute phase. These findings suggest that oligodendroglia-specific *Cx47* loss can augment inflammation upon autoimmune demyelination, underscoring a role for Cx47 in neuroinflammation.

Author contributions: Y.Z., R.Y., H.Y., H.U., K.M., M.W., T.M., N.I., and J.-i.K. designed research; Y.Z., R.Y., H.Y., S.N., H.U., Y.C., K.M., Y.N., K.I., M.W., T.M., N.I., and J.-i.K. performed research; H.Y. and H.U. contributed new reagents/analytic tools; Y.Z., R.Y., H.Y., H.U., Y.C., K.M., K.I., M.W., T.M., N.I., and J.-i.K. analyzed data; Y.Z., R.Y., H.Y., K.I., M.W., T.M., and J.-i.K. wrote the paper; and S.N. and Y.N. performed experiments for revision.

Competing interest statement: R.Y. has received honoraria from Biogen Japan; N.I. has received grant support from Mitsubishi Tanabe Pharma, Bayer Yakuhin Ltd., and Japan Blood Products Organization. J.-i.K. is a consultant for Biogen Japan and Medical Review, and has received honoraria from Bayer Healthcare, Mitsubishi Tanabe Pharma, Nobelpharma, Otsuka Pharmaceutical, Sanofi K.K., Chugai Pharmaceutical Co. Ltd., Teijin Pharma, Novartis Pharma, and Medical Review. The remaining authors declare no conflicts of interest.

This article is a PNAS Direct Submission.

Data deposition: The gene array results were uploaded to the Gene Expression Omnibus repository (accession no. GSE121339) on the National Center for Biotechnology Information homepage (https://www.ncbi.nlm.nih.gov/geo/query/acc.cgi?acc=GSE121339).

[1]To whom correspondence may be addressed. Email: kira@neuro.med.kyushu-u.ac.jp.

This article contains supporting information online at https://www.pnas.org/lookup/suppl/doi:10.1073/pnas.1901294117/-/DCSupplemental.

First published January 13, 2020.

sheaths in the white and gray matters (9, 10). Cx47 forms homotypic oligodendroglia–oligodendroglia GJs with itself, heterotypic oligodendroglia–oligodendroglia GJs with Cx32, and most heterotypic oligodendroglia–astroglia GJs with Cx43 (9, 11). *Cx47* mutations are a cause of Pelizaeus–Merzbacher-like disease, an autosomal recessive hypomyelinating leukoencephalopathy (12). However, single KO of *Cx47* in mice produced neither neurological signs nor demyelination in the spinal cord (13, 14). Here, we report that oligodendroglia-specific conditional ablation of *Cx47* augments neuroinflammation without influencing encephalitogenic T cell induction, producing relapsing EAE with florid microglial activation.

Results

_Cx47_ icKO Decreases Cx47 Expression in the White Matter Oligodendroglia. To confirm $CreER^T$-mediated recombination, *PLP/*$CreER^T$*;Rosa26-lacZ* reporter mice were injected with tamoxifen (TM) following a defined protocol (*SI Appendix*, Fig. S1*A*) and analyzed by X-gal staining (*SI Appendix*, Fig. S1 *B–D*). X-gal–positive cells were mainly observed in the white matter of the brain and whole-mount preparations of the spinal cord in TM-induced double-transgenic mice, as clearly shown by the strong X-gal staining in brain and spinal cord cross-sections. By contrast, no X-gal staining was observed in corn oil-injected double-transgenic control mice.

Next, we generated *PLP/*$CreER^T$*;Cx47*$^{fl/fl}$ mice (*SI Appendix*, Fig. S2) to achieve inducible conditional ablation of *Cx47*, wherein *Cx47* is ablated from oligodendroglia after TM injections according to the protocol (*SI Appendix*, Fig. S1*A*). TM-treated *PLP/*$CreER^T$*;Cx47*$^{fl/fl}$ mice are designated *Cx47* icKO mice hereafter. Double immunostaining for Cx47 and Nogo-A revealed that Cx47 was predominantly present in the oligodendroglia distributed in the white matter of the lumbar spinal cord (*SI Appendix*, Fig. S3*A*), consistent with a previous report (13). Compared with corn oil-injected control mice, Cx47 levels were significantly reduced in the spinal cord white matter of *Cx47* icKO mice at 10, 28, and 60 d after completion of TM injections (*SI Appendix*, Fig. S3*B*). Similar depletion of Cx47 was observed in the cerebellum and optic nerve white matter at 10, 28, and 60 d after completion of TM injections (*SI Appendix*, Fig. S3 *C* and *D*). Western blotting revealed that Cx47 gradually decreased at 10, 14, and 21 d after completion of TM injections, with a significant reduction at 28 d (*SI Appendix*, Fig. S3 *E* and *F*). We also confirmed that TM injection caused neither clinical signs nor histological changes, including myelin density alterations determined by myelin basic protein (MBP) immunostaining and inflammatory infiltrates, in *Cx47* icKO mice at time points corresponding to the acute and chronic phases of EAE (*SI Appendix*, Fig. S4).

Oligodendroglia-Specific _Cx47_ Ablation Aggravates Acute and Chronic EAE Signs. EAE was induced in 12- to 16-wk-old female mice by myelin oligodendrocyte glycoprotein $(MOG)_{35–55}$ peptide according to the protocol (*SI Appendix*, Fig. S5). We initially examined the effects of TM alone on EAE in *Cx47* fl/fl mice, because TM was reported to reduce the severity of acute EAE (15) through its immunosuppressive effects as an estrogen receptor modulator (16). TM injection significantly reduced the severity of clinical signs in acute (day postimmunization [dpi] 0 to 29) but not chronic (dpi 30 to 60) EAE and decreased inflammatory cell infiltrates and demyelination at the acute EAE phase only (*SI Appendix*, Fig. S6), consistent with the observation that TM was completely degraded within 8 d in mice (17). Therefore, throughout the following experiments, *Cx47* icKO and *Cx47* fl/fl mice were equally treated with TM to clarify the effects of *Cx47* ablation alone.

EAE eventually developed in all immunized mice. *Cx47* icKO mice showed tail and hind limb paresis similar to *Cx47* fl/fl mice at both the acute and chronic phases of EAE, with the overall disease severity being relatively mild because of the immunosuppressive effects of TM (15, 16). Compared with *Cx47* fl/fl mice, *Cx47* icKO mice showed significantly earlier onset, and higher acute phase peak scores, relapse numbers, and areas under the curve (AUCs) for clinical scores at both the acute (dpi 0 to 29) and chronic (dpi 30 to 72) phases of EAE (Fig. 1).

Oligodendroglia-Specific _Cx47_ Ablation Exacerbates Demyelination. In *Cx47* icKO mice, the myelin density determined by MBP immunostaining was significantly decreased at the acute and chronic phases of EAE compared with the preimmunized phase in both the ventral and dorsal funiculi of the spinal cord (Fig. 2*A* and *SI Appendix*, Fig. S7). By contrast, *Cx47* fl/fl mice showed no significant decreases in myelin density at the acute to chronic phases of EAE in either the ventral or dorsal funiculus, except for a significant decrease in the ventral funiculus at the chronic phase compared with the preimmunized phase. As a result, myelin loss was significantly more severe in *Cx47* icKO mice than in *Cx47*

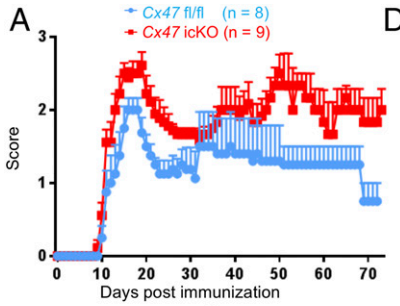

D

Comparisons of clinical features of EAE between *Cx47* icKO and *Cx47* fl/fl mice

Group	*Cx47* fl/fl (n = 17)	*Cx47* icKO (n = 16)	*P* value
Incidence	17/17 (100%)	16/16 (100%)	*n.s.*
Disease onset	10.94 ± 0.67	9.2 ± 1.97	0.04
Acute phase peak score	2.15 ± 0.09	2.81 ± 0.11	< 0.0001
Relapsed mouse number (%)	5/17 (29%)	9/16 (56%)	*n.s.*
Relapse numbers (average)	5/17 (0.29)	13/16 (0.81)	0.003

The sums of three independent experiments are shown. *n.s.* = not significant.

Fig. 1. Aggravation of EAE by oligodendroglia-specific *Cx47* ablation. (*A*) Clinical scores in *Cx47* fl/fl control (blue; $n = 8$) and *Cx47* icKO (red; $n = 9$) mice. (*B* and *C*) Severity of disease symptoms evaluated by comparing the AUC values (*B*) from dpi 0 to dpi 29 (acute phase, 8 *Cx47* fl/fl mice vs. 9 *Cx47* icKO mice) and (*C*) from dpi 30 to dpi 72 (chronic phase, 5 *Cx47* fl/fl mice vs. 6 *Cx47* icKO mice). (*D*) Comparisons of clinical features of EAE between *Cx47* icKO and *Cx47* fl/fl mice. The sums of three independent experiments are shown. All data are shown as means ± SEM. *P* values were calculated by the Mann–Whitney *U* test. ***$P < 0.001$.

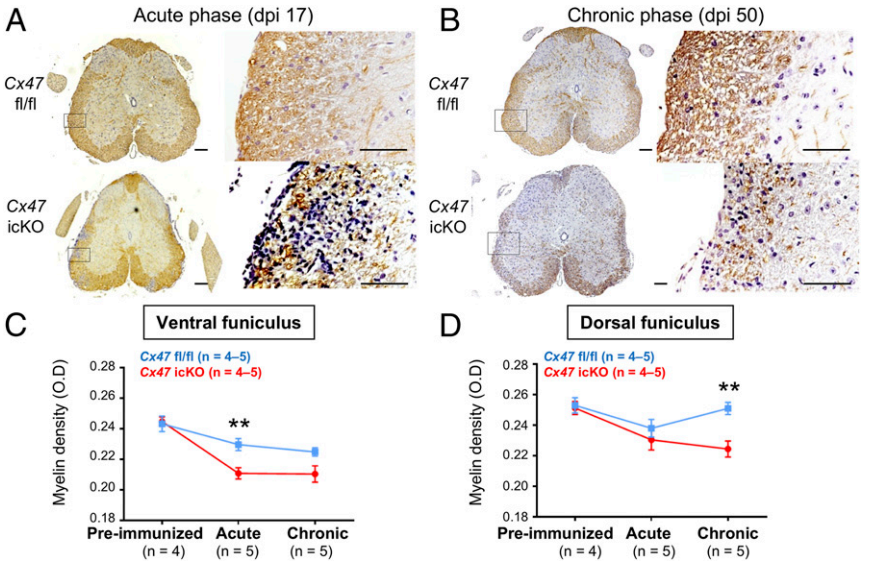

Fig. 2. Exacerbation of demyelination by oligodendroglia-specific *Cx47* ablation. (*A* and *B*) MBP immunostaining of lumbar spinal cords (counterstained with DAPI) from *Cx47* fl/fl (*Upper*) and *Cx47* icKO (*Lower*) EAE mice at (*A*) dpi 17 and (*B*) dpi 50. Magnified images of the boxed areas in *Left* are shown in *Right*. (Scale bars: *Left*, 100 μm; *Right*, 10 μm.) (*C* and *D*) Quantitative analysis of myelin densities using optimal density measurements in the (*C*) ventral and (*D*) dorsal funiculi of the lumbar spinal cord from *Cx47* fl/fl and *Cx47* icKO mice by MBP immunostaining. All data are presented as means ± SEM. Significant differences were determined by one-way analysis of variance (ANOVA). $^{**}P < 0.01$.

fl/fl mice in the ventral funiculus at the acute phase ($P = 0.009$) and in the dorsal funiculus at the chronic phase ($P = 0.005$), while the myelin density was unchanged between the two genotypes in the preimmunized phase.

Oligodendroglia-Specific *Cx47* Ablation Augments T Cell and Macrophage Infiltration at the Acute EAE Phase. Neuroinflammation was strongest in the L4 to L5 spinal cord among the CNS tissues, while other sites examined (cerebrum, cerebellum, and brainstem) contained only a few inflammatory foci in both genotypes (Fig. 3 and *SI Appendix*, Fig. S8). More infiltration of $CD3^+$ T cells was observed in *Cx47* icKO mice compared with *Cx47* fl/fl mice in the ventral and dorsal funiculi of the spinal cord at both the acute and chronic phases (ventral funiculus: acute, $P = 0.003$ and chronic, $P = 0.02$; dorsal funiculus: acute, $P = 0.01$ and chronic, $P = 0.02$) (Fig. 3 *A–C*). Iba-1^+ microglia were more abundant in the ventral funiculus of the spinal cord in *Cx47* icKO mice than in *Cx47* fl/fl mice at both the acute and chronic phases (acute, $P = 0.02$ and chronic, $P = 0.04$) (Fig. 3 *D–F*), while no significant changes were detected in the dorsal funiculus between the two genotypes. $F4/80^+$ macrophages showed increased infiltration in the ventral funiculus of the spinal cord in *Cx47* icKO mice compared with *Cx47* fl/fl mice at the acute phase ($P = 0.03$), with similar, but nonsignificant, trends observed in the acute dorsal and chronic ventral funiculi (*SI Appendix*, Fig. S9 *A–C*). Glial fibrillary acidic protein $(GFAP)^+$ astroglia showed no significant changes in either the ventral or dorsal funiculus of the spinal cord in *Cx47* icKO mice compared with *Cx47* fl/fl mice at the acute and chronic phases, except for a significant increase in the dorsal funiculus at the chronic phase in *Cx47* icKO mice (*SI Appendix*, Fig. S9 *D–F*). Furthermore, myelin density showed significant negative correlations with extents of $CD3^+$ T cell and Iba-1^+ microglia infiltration in the ventral and dorsal funiculi of the lumbar spinal cord at both the acute and chronic phases in *Cx47* icKO mice (*SI Appendix*, Figs. S10 and S11). Similar, but nonsignificant, trends were observed in *Cx47* fl/fl mice.

MOG-Specific T Cell Response Is Unaltered in *Cx47* icKO Mice. Splenocytes isolated from *Cx47* icKO and *Cx47* fl/fl mice at the preonset (dpi 10) and peak (dpi 17) phases of EAE were stimulated by different concentrations of $MOG_{35–55}$. There were no significant differences in MOG-specific proliferation between the two genotypes at both time points (*SI Appendix*, Fig. S12 *A* and *B*). Furthermore, the amounts of interleukin (IL)-2, IL-3, IL-4, IL-5, IL-6, IL-10, IL-17, interferon (IFN)-γ, and C-C motif chemokine 2 (CCL2) secreted by splenocytes into the supernatant upon MOG stimulation at dpi 17 did not differ significantly between *Cx47* icKO and *Cx47* fl/fl mice (*SI Appendix*, Fig. S12*C*).

Decrease in Oligodendroglial Cx47 at the Peak of Acute EAE. The alterations in oligodendroglial Cx47 were immunohistochemically examined in the lumbar spinal cord at the acute and chronic phases of EAE in WT mice on the same genetic background (C57BL/6) as *Cx47* icKO and *Cx47* fl/fl mice. In the preimmunized phase, Cx47 was expressed in the perikarya and proximal processes of oligodendroglia as previously reported (17, 18). Cx47 expression started to decrease at the preonset phase, albeit without significance, and was further down-regulated from dpi 8 to 14 with significance (*SI Appendix*, Fig. S13). At the chronic phase (dpi 50), Cx47 expression was partially recovered, consistent with a previous report (7). In *Cx47* fl/fl mice, Cx47 expression was significantly reduced at the acute EAE peak compared with the preimmunized phase ($P < 0.0001$), and partially recovered at the chronic phase (acute vs. chronic phases, $P = 0.0057$) but remained lower than that in the preimmunized phase ($P = 0.0027$) (*SI Appendix*, Fig. S14). Although Cx47 expression levels were extremely low in *Cx47* icKO mice, they were significantly decreased at the acute phase compared with the preimmunized phase ($P = 0.0025$), and then recovered to similar levels to the preimmunized phase at the chronic phase. As a result, Cx47 levels were significantly lower in the preimmunized and chronic phases compared with *Cx47* fl/fl mice ($P < 0.0001$ for both), while the difference was not significant at the peak of EAE, due to the floor effects.

No Changes in Astroglial Cx43 Expression in *Cx47* icKO Mice. Cx43 expression was significantly decreased at the acute phase in both *Cx47* icKO and *Cx47* fl/fl mice compared with the preimmunized phase ($P = 0.0002$ and $P = 0.0014$, respectively), and recovered to levels similar to the preimmunized phase at the chronic phase (*SI Appendix*, Fig. S15). Thus, there was no significant difference

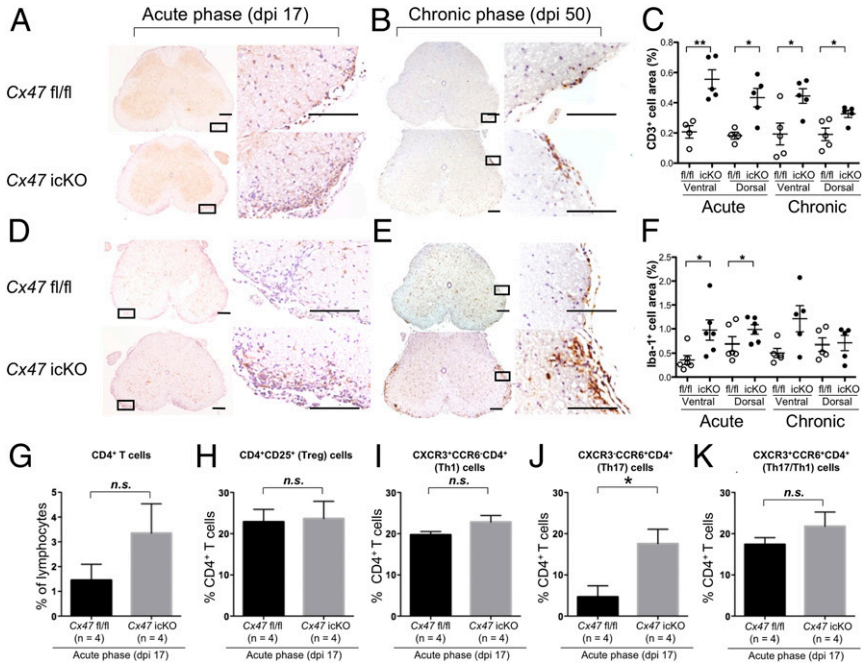

Fig. 3. Augmentation of T cell infiltration and activation of microglia during EAE by oligodendroglia-specific *Cx47* ablation. (*A*, *B*, *D*, and *E*) Immunohistochemical staining of lumbar spinal cords (counterstained with DAPI) from *Cx47* fl/fl (*Upper*) and *Cx47* icKO (*Lower*) mice at the (*A* and *D*) acute (dpi 17) and (*B* and *E*) chronic (dpi 50) phases of EAE. Immunostaining of (*A* and *B*) $CD3^+$ T cells and (*D* and *E*) Iba-1^+ microglia is shown. (Scale bars: *Left*, 100 μm; *Right*, 10 μm.) (*C* and *F*) Quantitative analysis of (*C*) $CD3^+$ T cells and (*F*) Iba-1^+ microglia in the ventral and dorsal funiculi of lumbar spinal cords from *Cx47* icKO and *Cx47* fl/fl mice at dpi 17 and dpi 50. Open circle and filled circle in *C* and *F* indicate fl/fl and icKO, respectively. (*G*–*K*) Bar graphs showing the percentages of (*G*) $CD4^+$ T, and (*H*) Treg, (*I*) Th1, (*J*) Th17, and (*K*) Th17/Th1 cells in $CD4^+$ T cells isolated from *Cx47* fl/fl and *Cx47* icKO mouse CNS tissues by flow cytometry. All data are shown as means ± SEM of four to seven mice per group. Significant differences were determined by an unpaired *t* test. $*P < 0.05$; $**P < 0.01$; *n.s.*, not significant.

in Cx43 immunoreactivity in the lumbar spinal cord white matter between *Cx47* icKO and *Cx47* fl/fl mice in the preimmunized phase and during the course of EAE.

Oligodendroglia-Specific *Cx47* Ablation Promotes Astroglia toward the A1 Phenotype at the Acute EAE Phase. First, we compared the changes in expression of gene clusters among the preimmunized, acute, and chronic phases by gene set enrichment analysis (GSEA) in *Cx47* icKO and *Cx47* fl/fl mice. Compared with the preimmunized phase, expression levels of A1-specific (induced by neuroinflammation), A2-specific (induced by ischemia), and Pan-reactive (induced by both neuroinflammation and ischemia) genes (18) were significantly greater in both mutant and control mice at the acute phase (*Cx47* icKO: A1 and Pan, normalized $P < 0.001$ and A2, normalized $P = 0.018$; *Cx47* fl/fl: A1, normalized $P = 0.017$, A2, normalized $P = 0.0226$, and Pan, normalized $P < 0.001$) (*SI Appendix*, Table S1 and Fig. 4*A*). In the comparison between the preimmunized and chronic phases, A1-specific gene expression levels were significantly enhanced at the chronic phase only in *Cx47* icKO mice (A1, normalized $P = 0.005$), but not in *Cx47* fl/fl mice, while no difference was observed in A2-specific and Pan-reactive gene expression levels in both genotypes (*SI Appendix*, Table S1). Compared with the acute phase, A1-specific, A2-specific, and Pan-reactive gene expression levels showed significant down-regulation at the chronic phase in both genotypes (*SI Appendix*, Table S1).

Next, we compared the changes in expression of gene clusters between the two mouse genotypes during the EAE disease course by GSEA. At the acute phase, *Cx47* icKO mice showed higher expression levels of A1-specific and Pan-reactive genes than *Cx47* fl/fl mice (normalized $P = 0.004$ and $P = 0.014$, respectively), while A2-specific gene expression was similar between the two genotypes (*SI Appendix*, Table S2 and Fig. 4*B*). At the chronic phase, no significant changes in A1-specific, A2-specific, and Pan-reactive gene expression levels were found between the two genotypes.

We immunohistochemically examined the expressions of representative A1 and A2 astroglia markers based on a recent report (18), and found a significant increase in $GFAP^+$ astroglia expressing C3, a representative A1 marker, in the lumbar spinal cord white matter of *Cx47* icKO mice compared with *Cx47* fl/fl mice at both the acute and chronic phases ($P = 0.006$ and $P = 0.014$, respectively) (Fig. 5 *A* and *E* and *SI Appendix*, Fig. S16 *A* and *E*). No significant change in $GFAP^+$ astroglia expressing S100A10, a representative A2 marker, was found in *Cx47* icKO mice compared with *Cx47* fl/fl mice at the acute phase, while $S100A10^+$ astroglia were significantly more abundant in *Cx47* icKO mice than in *Cx47* fl/fl mice at the chronic phase ($P = 0.028$) (Fig. 5 *C* and *F* and *SI Appendix*, Fig. S16 *B* and *F*).

Oligodendroglia-Specific *Cx47* Ablation Dampens Oligodendroglia-Specific Gene Expression at the Acute EAE Phase. Compared with the preimmunized phase, expression levels of the top 30 oligodendroglia-specific genes were significantly down-regulated in both genotypes at the acute phase by GSEA (*Cx47* icKO and *Cx47* fl/fl, normalized $P < 0.001$ for both) (*SI Appendix*, Table S1 and Fig. S16). At the chronic phase, oligodendroglia-specific gene expressions were further down-regulated compared with the acute and preimmunized phases in both genotypes (compared with acute phase: *Cx47* icKO, normalized $P = 0.007$ and *Cx47* fl/fl, normalized $P < 0.001$; compared with preimmunized phase: *Cx47* icKO and *Cx47* fl/fl, normalized $P < 0.001$ for both). Next, we compared the expression levels of oligodendroglia-specific gene clusters between the two genotypes during the EAE disease course by GSEA. At the acute phase, oligodendroglia-specific gene clusters were significantly down-regulated in *Cx47* icKO mice compared with *Cx47* fl/fl mice ($P = 0.014$) (*SI Appendix*, Table S2 and Fig. S17). At the chronic phase, higher oligodendroglia-specific gene expression

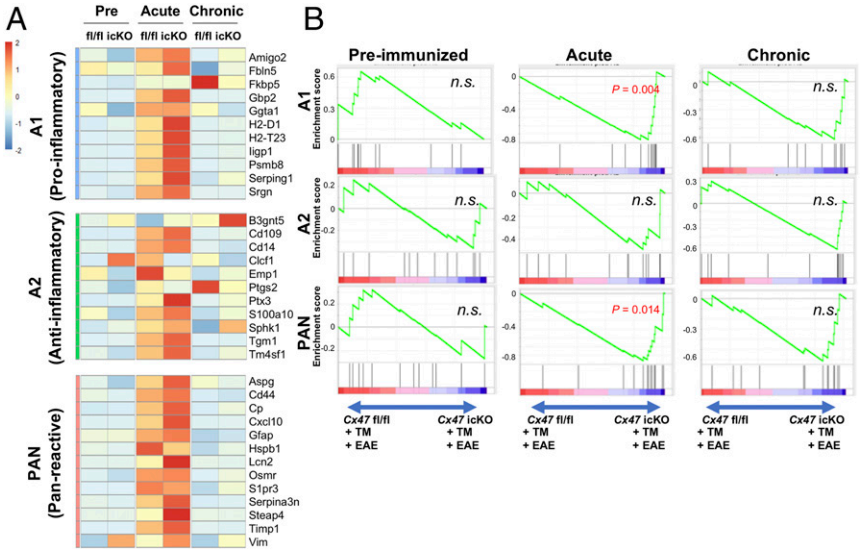

Fig. 4. Gene expression microarray data for *Cx47* icKO and *Cx47* fl/fl mouse spinal cord and brain in the preimmunized and EAE phases focusing on astroglia-related genes. (*A*) Heat maps comparing the expression of A1-specific, A2-specific, and Pan-reactive gene transcripts in RNA samples from the spinal cord and brain of *Cx47* icKO and *Cx47* fl/fl mice ($n = 3$ per group) in the preimmunized, acute (dpi 17), and chronic (dpi 50) phases of EAE. To create the heat maps, the original mRNA signal values were subjected to $\log_2$ transformation, and the distance from the median value (control) of each gene was calculated. The numbers −2 to 2 beside the color bar indicate $\log_2$-transformed fold changes, reflecting fold differences in gene expression from less than 1/4 to more than 4, respectively. (*B*) Enrichment plots (green curves) show the running sums of the enrichment score (ES) for A1-specific, A2-specific, and Pan-reactive gene sets in the preimmunized, acute, and chronic phases of EAE. The score at the peak of each plot is the ES for that gene set. The black bars indicate where the members of the gene set appear in the ranked list of genes. A predominance of black bars to the left or right side indicates that most genes are up-regulated in *Cx47* fl/fl or *Cx47* icKO EAE mice, respectively. n.s., not significant.

levels were found in *Cx47* icKO mice compared with *Cx47* fl/fl mice ($P < 0.001$).

Oligodendroglia-Specific *Cx47* Ablation Promotes Microglia to Differentiate toward the Proinflammatory Phenotype at the Acute and Chronic Phases of EAE. First, we compared the changes in expression levels of proinflammatory and antiinflammatory genes in isolated microglia among the preimmunized, acute, and chronic phases in *Cx47* icKO and *Cx47* fl/fl mice by GSEA (19). Compared with the preimmunized phase, proinflammatory and antiinflammatory gene expression levels in microglia were significantly higher in both genotypes at the acute phase (*Cx47* icKO: normalized $P < 0.001$ for both proinflammatory and antiinflammatory genes; *Cx47* fl/fl: normalized $P < 0.001$ for proinflammatory genes and normalized $P = 0.0022$ for antiinflammatory genes) (*SI Appendix*, Table S1 and Fig. 6*A*). At the chronic phase, proinflammatory gene expression levels in microglia only remained significantly up-regulated compared with the preimmunized phase in *Cx47* icKO mice (*Cx47* icKO: normalized $P = 0.049$), and not in *Cx47* fl/fl mice, while antiinflammatory gene expression levels were significantly greater than those in the preimmunized phase in both genotypes (*Cx47* icKO: normalized $P < 0.001$; *Cx47* fl/fl: normalized $P = 0.0065$).

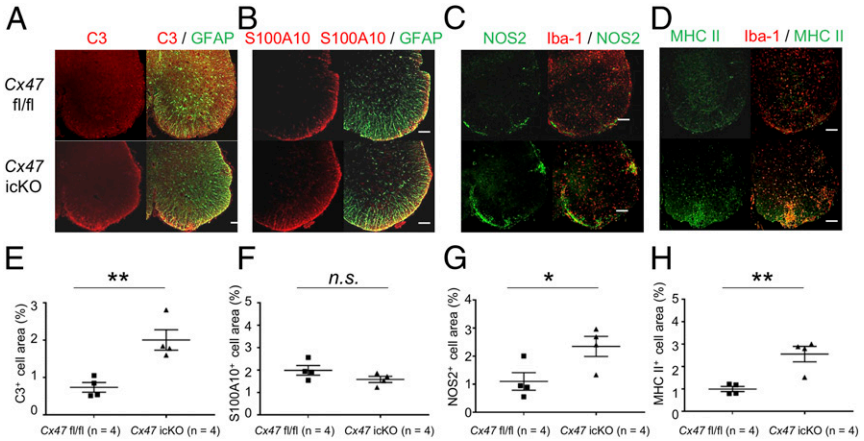

Fig. 5. Immunohistochemistry for representative A1 and A2 astroglia markers in GFAP$^+$ astroglia, and NOS2 and MHC class II molecules in Iba-1$^+$ microglia at the acute phase of EAE. (*A–D*) Double immunostaining for (*A*) C3 (red) and GFAP (green), (*B*) S100A10 (red) and GFAP (green), (*C*) NOS2 (red) and Iba1 (green), and (*D*) MHC class II molecules (red) and IBa1 (green) in lumbar spinal cords from *Cx47* fl/fl control (*Upper*) and *Cx47* icKO (*Lower*) mice at the acute phase of EAE (dpi 17). (Scale bars: 100 μm.) (*E–H*) Quantitative analysis of (*E*) C3$^+$ and (*F*) S100A10$^+$ astroglia and (*G*) NOS2$^+$ and (*H*) MHC class II$^+$ microglia in lumbar spinal cords from *Cx47* fl/fl and *Cx47* icKO mice at the acute phase of EAE. All data are shown as means ± SEM of four mice per group. Significant differences were determined by an unpaired *t* test. $^*P < 0.05$; $^{**}P < 0.01$. *n.s.*, not significant.

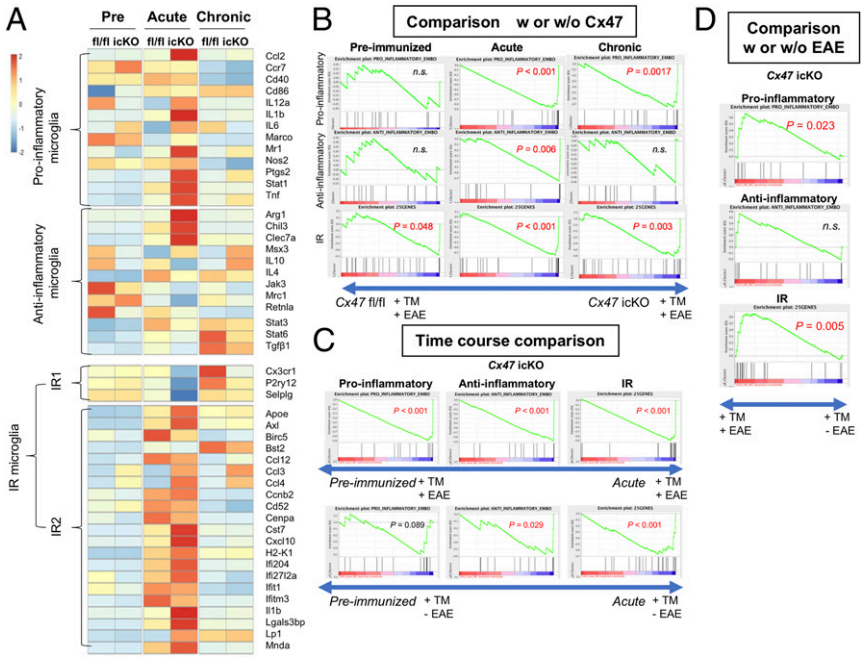

Fig. 6. Proinflammatory, antiinflammatory, and IR-related gene expressions in microglia isolated from the spinal cord and brain of *Cx47* fl/fl and *Cx47* icKO mice by microarray analysis. (*A*) Heat maps comparing the mean expression of proinflammatory, antiinflammatory, IR1-related, and IR2-related gene transcripts in RNA samples from microglia isolated from spinal cord and brain tissues of *Cx47* fl/fl and *Cx47* icKO mice ($n = 3$ per group) in the preimmunized, acute (dpi 17), and chronic (dpi 50) phases of EAE. The numbers −2 to 2 beside the color bar indicate $\log_2$-transformed fold changes, reflecting fold differences in gene expression from less than 1/4 to more than 4, respectively. (*B*) Enrichment plots (green curves) showing the running sums of the ES for proinflammatory, antiinflammatory, and IR-related gene sets in the preimmunized, acute, and chronic phases of EAE. The score at the peak of each plot is the ES for that gene set. The black bars indicate where the members of the gene set appear in the ranked list of genes. A predominance of black bars to the left or right side indicates that most genes are up-regulated in *Cx47* fl/fl or *Cx47* icKO EAE mice. (*C*) Time course comparison of proinflammatory, antiinflammatory, and IR-related gene sets between time points corresponding to the preimmunized phase and acute phase (dpi 17) in TM-injected *Cx47* icKO mice with and without EAE by GSEA. (*D*) Comparison of proinflammatory, antiinflammatory, and IR-related gene sets between TM-injected *Cx47* icKO mice with and without EAE by GSEA at the time point corresponding to the acute phase (dpi 17); w, with; w/o, without. *n.s.*, not significant.

Next, we compared the changes in proinflammatory and antiinflammatory gene expression levels in microglia between the two genotypes during the EAE disease course by GSEA. No significant differences in the expression levels of either proinflammatory or antiinflammatory genes in microglia were found in the preimmunized phase between *Cx47* icKO and *Cx47* fl/fl mice, while expressions of both proinflammatory and antiinflammatory genes were highly significantly enriched in *Cx47* icKO microglia compared with *Cx47* fl/fl microglia at the acute phase (proinflammatory genes: normalized $P < 0.001$; antiinflammatory genes: normalized $P = 0.006$) (*SI Appendix*, Table S2 and Fig. 6*B*). However, at the chronic phase, expressions of proinflammatory, but not antiinflammatory, genes were significantly higher in *Cx47* icKO microglia than in *Cx47* fl/fl microglia ($P = 0.0017$).

Given a recent report that injury-response (IR) microglia were induced by injection of demyelinating agent lysolecithin into the subcortical white matter (20), we compared the changes in IR-related gene expressions among the preimmunized, acute, and chronic phases in the two genotypes by GSEA. Compared with the preimmunized phase, expression levels of IR-related genes were significantly up-regulated in both mutant and control mice at the acute phase (*Cx47* icKO and *Cx47* fl/fl: normalized $P < 0.001$ for both) (*SI Appendix*, Table S1). In comparisons between the preimmunized and chronic phases, IR-related gene expressions remained up-regulated at the chronic phase in both genotypes (*Cx47* icKO and *Cx47* fl/fl: normalized $P < 0.001$ for both) (*SI Appendix*, Table S1). Compared with the acute phase, IR-related gene expression levels showed significant down-regulation in *Cx47* fl/fl mice at the chronic phase (normalized $P = 0.004$), but only marginally significant down-regulation in *Cx47* icKO mice (normalized $P = 0.0579$) (*SI Appendix*, Table S1).

Next, we compared IR-related gene expression levels between the two genotypes during the EAE disease course by GSEA. The results revealed that, even in the preimmunized phase, microglia isolated from *Cx47* icKO mice expressed IR-related genes significantly more abundantly than those from *Cx47* fl/fl mice ($P = 0.048$) (*SI Appendix*, Table S2 and Fig. 6*B*). At the acute and chronic phases, IR-related gene expressions were highly enriched in *Cx47* icKO mice compared with *Cx47* fl/fl mice ($P < 0.001$ for both acute and chronic phases). We further compared the expression levels of IR-related gene clusters, comprising IR1-related (canonical microglial markers) and IR2-related (IFN response genes) clusters, which were reported to behave reciprocally (20), between the two genotypes during the EAE disease course. Our heat map analysis revealed that IR1-related and IR2-related genes did indeed show reciprocal behavior at the acute and chronic phases, with IR2-related gene clusters being more abundantly expressed at the acute phase in both genotypes, especially *Cx47* icKO mice, and IR1-related gene clusters being more enriched at the chronic phase in both genotypes, especially *Cx47* fl/fl mice (Fig. 6*A*). These findings indicate pronounced activation of IR2-type microglia, demonstrating up-regulation of a variety of proinflammatory cytokine/chemokine genes, including *Il1b*, *Ccl3*, *Ccl4*, and *Cxcl10*, in *Cx47* icKO mice at the preimmunized phase and more pronounced up-regulation at the acute and chronic EAE phases.

Subsequently, we performed a time course comparison between the preimmunized phase and a time point corresponding to the acute EAE phase (dpi 17) in TM-injected *Cx47* icKO mice

with and without EAE by GSEA (Fig. 6*C*). At dpi 17, TM-injected *Cx47* icKO mice with EAE showed up-regulation of all gene clusters compared with the preimmunized phase ($P < 0.001$ for proinflammatory, antiinflammatory, and IR-related), while mice without EAE showed up-regulation of antiinflammatory and IR-related gene clusters ($P = 0.029$ and $P < 0.001$, respectively), but not proinflammatory gene clusters ($P = 0.089$). The comparison between TM-injected *Cx47* icKO mice with and without EAE at dpi 17 to clarify the effects of EAE on the gene clusters revealed significant increases in both proinflammatory and IR-related gene clusters ($P = 0.0023$ and $P = 0.005$, respectively), but not antiinflammatory gene clusters ($P = 0.19$) (Fig. 6*D*). These findings suggest that TM injection followed by *Cx47* ablation without EAE enhances antiinflammatory and IR-related gene expressions at the time point corresponding to the acute phase, while proinflammatory and IR-related gene clusters are more profoundly up-regulated by EAE induction in TM-injected *Cx47* icKO mice.

We immunohistochemically examined the expressions of representative proinflammatory and antiinflammatory gene products in Iba-1$^+$ microglia. At the acute phase, significant increases in immunoreactivity for nitric oxide synthase 2 (NOS2), a representative proinflammatory marker, and arginase 1 (Arg-1), a representative antiinflammatory marker, were observed in Iba-1$^+$ microglia in *Cx47* icKO mice compared with *Cx47* fl/fl mice (NOS2, $P = 0.039$; Arg-1, $P = 0.044$) (Fig. 5 *C* and *G* and *SI Appendix*, Fig. S18 *A* and *B*). At the chronic phase, a significant increase in immunoreactivity for NOS2 was found in Iba-1$^+$ microglia in *Cx47* icKO mice compared with *Cx47* fl/fl mice ($P = 0.014$) (Fig. 5 *C* and *G*), while similar levels of immunoreactivity for Arg-1 were observed between the two genotypes (*SI Appendix*, Fig. S18 *C* and *D*).

Oligodendroglia-Specific *Cx47* Ablation Up-Regulates Microglial Expression of Major Histocompatibility Complex Genes in the Acute Phase of EAE. As major histocompatibility complex (MHC) molecules play key roles in relevant antigen presentation to T cells, we examined MHC-related gene expressions in isolated microglia by microarray analysis. MHC-related genes were mainly up-regulated at the chronic phase in both *Cx47* icKO and *Cx47* fl/fl mice, while, interestingly, one gene cluster including MHC class II genes like *H2-Aa*, *H2-Ab1*, and *H2-Eb1* was markedly up-regulated in *Cx47* icKO mice compared with *Cx47* fl/fl mice at the acute phase (*SI Appendix*, Fig. S19*A*). According to the GSEA results, *Cx47* icKO mice had significantly more up-regulated MHC-related gene expressions than *Cx47* fl/fl mice at the acute phase ($P < 0.001$) (*SI Appendix*, Fig. S19*B*). The MHC-related gene expressions in *Cx47* icKO microglia also tended to be increased at the preimmunized phase ($P = 0.051$), but not at the chronic phase.

By immunohistochemistry, we confirmed that *Cx47* icKO mice had significantly more Iba-1$^+$ microglia expressing MHC class II molecules than *Cx47* fl/fl mice at the acute phase ($P = 0.005$) (Fig. 5 *D* and *H*). Even at the chronic phase, Iba-1$^+$ microglia expressing MHC class II molecules tended to be more abundant in *Cx47* icKO mice than in *Cx47* fl/fl mice, although the difference was not significant (*SI Appendix*, Fig. S16 *D* and *H*). Moreover, genes in one of the complement clusters (*Serping1*, *C3*, *C4b*, *C2*, *C1qc*, *Cd93*, and *A2m*) were significantly up-regulated in *Cx47* icKO mice compared with *Cx47* fl/fl mice at the acute phase, although the overall expression of complement-related genes did not differ significantly between the two genotypes (*SI Appendix*, Fig. S20).

Oligodendroglia-Specific *Cx47* Ablation Enriches Genes Related to Innate Immune and Inflammatory Pathways in Microglia at the Acute and Chronic EAE Phases. The gene expression data for isolated microglia were subjected to Gene Ontology (GO) enrichment analysis using the Database for Annotation, Visualization and Integrated Discovery (DAVID). In the preimmunized phase, the differentially expressed genes (DEGs) between *Cx47* icKO and *Cx47* fl/fl mice microglia were enriched in neutrophil chemotaxis, inflammatory response, and chemokine-related GO terms (*SI Appendix*, Fig. S21*A*). At the acute and chronic phases of EAE, the DEGs between *Cx47* icKO and *Cx47* fl/fl mice microglia were enriched in inflammatory response, innate immune response, neutrophil chemotaxis, monocyte chemotaxis, and leukocyte migration GO terms (*SI Appendix*, Table S3 and Fig. S21 *B* and *C*). Notably, the DEGs between *Cx47* icKO and *Cx47* fl/fl microglia were markedly enriched in inflammatory response GO terms in the preimmunized and EAE phases, suggesting that *Cx47* ablation renders microglia more proinflammatory in the preimmunized phase as well as the acute to chronic phases of EAE. We further analyzed the functional pathways using only up-regulated genes (*SI Appendix*, Fig. S22). The results using up-regulated DEGs between *Cx47* icKO and *Cx47* fl/fl microglia were essentially the same as those using all DEGs.

Oligodendroglia-Specific *Cx47* Ablation Causes More Dysregulation in Proinflammatory Gene Expressions in CNS Tissues at the Acute and Chronic EAE Phases. Compared with *Cx47* fl/fl mice, CNS tissues from *Cx47* icKO mice at the acute phase exhibited dysregulation of antigen processing and presentation, phagosome, and cell adhesion pathways, where most involved genes were up-regulated, by a gene expression analysis with the Kyoto Encyclopedia of Genes and Genomes (KEGG) database (*SI Appendix*, Table S4 and Figs. S23 and S24). Even at the chronic phase, leukocyte transendothelial migration pathways were dysregulated in *Cx47* icKO mice, in which all involved genes were up-regulated (*SI Appendix*, Table S4 and Figs. S23 and S24). A calcium signaling pathway was also dysregulated at all clinical phases, including the preimmunized phase in *Cx47* icKO mice (*SI Appendix*, Table S4 and Fig. S25). These findings are compatible with aggravation of acute and chronic neuroinflammation in *Cx47* icKO mice. Next, we analyzed the KEGG pathways using only up-regulated genes (*SI Appendix*, Fig. S23). The results using the up-regulated DEGs between *Cx47* icKO and *Cx47* fl/fl microglia were essentially the same as those using all DEGs.

Oligodendroglia-Specific *Cx47* Ablation Facilitates Helper T 17 Cell Migration into CNS at the Acute EAE Phase. Although oligodendroglia-specific *Cx47* ablation did not significantly alter the percentages of total CD4$^+$ T cells in CNS-infiltrating lymphocytes between *Cx47* icKO and *Cx47* fl/fl mice by flow cytometry, CXCR3$^-$CCR6$^+$CD4$^+$ (helper T [Th] 17) cell percentages in CD4$^+$ T cells were significantly increased in *Cx47* icKO mice compared with *Cx47* fl/fl mice ($P = 0.026$), while CXCR3$^+$CCR6$^-$CD4$^+$ (Th1), CD4$^+$CD25$^+$ regulatory T (Treg), and CXCR3$^+$CCR6$^+$CD4$^+$ (Th17/Th1) cell percentages were not significantly changed (Fig. 3 *G*–*K* and *SI Appendix*, Fig. S27). Furthermore, the intracellular cytokine staining in isolated mononuclear cells from the CNS tissues revealed a significant increase in IL-17$^+$IFNγ$^-$CD4$^+$ T (Th17) cell percentages in *Cx47* icKO mice compared with *Cx47* fl/fl mice ($P = 0.0286$), but not in IL-17$^-$IFNγ$^+$CD4$^+$ T (Th1) or IL-17$^+$IFNγ$^+$CD4$^+$ T (Th17/Th1) cell percentages (*SI Appendix*, Fig. S28).

We then measured the chemokine expressions in isolated microglia from CNS tissues at the preimmunized and acute phases by microarray analysis (*SI Appendix*, Table S5 and Fig. S29*A*). Among them, *Ccl3* (ratio, 11.79), *Ccl2* (7.17), *Cxcl13* (6.38), *Ccl4* (3.92), *Cxcl9* (2.48), *Ccl8* (2.34), *Cxcl16* (2.41), *Ccl7* (2,111), *Cxcl10* (2.10), and *Cxcl2* (1.85) were significantly up-regulated in *Cx47* icKO mice compared with *Cx47* fl/fl mice at the acute phase. Because Th17 cells express not only CCR6 but also other chemokine receptors, such as CCR2 and CCR5 (21, 22), the expression of ligands for these Th17 cell chemokine receptors, that

is, CCL2, CCL7, and CCL8 for CCR2, and CCL3, CCL4, and CCL8 for CCR5, is suggested to be significantly increased in *Cx47* icKO mice compared with *Cx47* fl/fl mice. Thus, we measured the expressions of representative ligands for these chemokine receptors in isolated microglia from CNS tissues at the acute phase by RT-PCR. The levels of CCL2 were significantly increased ($P = 0.0322$), and those of CCL5 showed a tendency to increase ($P = 0.0986$) in *Cx47* icKO mice compared with *Cx47* fl/fl mice (*SI Appendix*, Fig. S29 *B* and *C*).

Effects of oligodendroglial Cx47 ablation on astroglia and microglia gene expressions after TM injection without EAE. Compared with the preimmunized phase, the expression levels of A1-specific and Pan-reactive genes were significantly greater at the acute phase in *Cx47* icKO mice with TM injection but without EAE (A1, normalized $P = 0.005$; Pan, normalized $P < 0.001$), but not in *Cx47* fl/fl mice with TM injection, while the A2-specific gene expression levels remained unchanged in both genotypes (*SI Appendix*, Table S6 and Fig. S30). Comparisons between the two genotypes revealed no significant changes in A1-specific, A2-specific, and Pan-reactive gene expression levels, except for enhancement of Pan-reactive gene expression levels at the acute phase time in *Cx47* icKO mice without EAE (normalized $P = 0.008$) (*SI Appendix*, Table S6 and Fig. S30).

Concerning microglia genes, expression levels of antiinflammatory and IR-related genes were significantly greater in both genotypes at the acute phase time point compared with the preimmunized phase time point (*Cx47* icKO with TM but without EAE: antiinflammatory, normalized $P = 0.03$ and IR-related, normalized $P < 0.001$; *Cx47* fl/fl with TM but without EAE: antiinflammatory, normalized $P = 0.007$ and IR-related, normalized $P < 0.001$), while the proinflammatory gene expression levels were unchanged in both genotypes (*SI Appendix*, Table S6 and Fig. S31). A comparison between the two genotypes revealed no significant differences in these gene expression levels except for a marginal increase in IR-related gene expression levels in *Cx47* icKO mice with TM but without EAE ($P = 0.048$) (*SI Appendix*, Table S6 and Fig. S31).

Net effects of oligodendroglial Cx47 ablation and TM injection on astroglia and microglia gene expressions without EAE. Finally, in the absence of EAE induction, *Cx47* icKO mice without TM injection at the preimmunized phase time point showed significantly higher A1-specific, A2-specific, and Pan-reactive gene expressions than *Cx47* icKO mice with TM injection (A1, normalized $P = 0.021$; A2, normalized $P < 0.001$; Pan, normalized $P = 0.041$) (*SI Appendix*, Table S7 and Fig. S32). At the acute phase time point, there were no differences between the two genotypes in A1-specific and A2-specific gene expressions whereas Pan-reactive gene expressions were greater in *Cx47* icKO mice with TM injection (*Cx47*-ablated) than in *Cx47* icKO mice without TM injection (*Cx47*-nonablated), reflecting the effects of *Cx47* ablation (*SI Appendix*, Table S7 and Fig. S32).

Regarding microglial genes, antiinflammatory and IR-related gene expression levels were significantly greater in *Cx47* icKO mice without TM injection than in those with TM injection (antiinflammatory, normalized $P = 0.012$; IR-related, normalized $P < 0.001$), but proinflammatory gene levels were unchanged at the preimmunized phase, probably because of the overwhelming immunosuppressive effects of TM (*SI Appendix*, Table S7 and Fig. S33). At the acute phase, no significant changes in proinflammatory and antiinflammatory gene expression levels in microglia were found between *Cx47* icKO mice with and without TM injection in the absence of EAE induction, while IR-related gene expressions were significantly higher in *Cx47* icKO mice with TM injection (*Cx47*-ablated) than those without TM injection (*Cx47*-nonablated) (normalized $P < 0.001$) (*SI Appendix*, Table S7 and Fig. S33). These findings suggest that the augmenting effects of *Cx47* ablation on Pan-reactive astroglial and IR-related microglial gene expressions become evident as the immunosuppressive effects of TM subside.

Discussion

The most important finding of the present study is that oligodendroglia-specific *Cx47* ablation is sufficient to induce severe neuroinflammation upon autoimmune demyelination, suggesting that exacerbation of acute and chronic EAE is not simply attributable to energy failure caused by loss of oligodendroglia–astroglia GJs but rather that Cx47 plays a critical role in controlling neuroinflammation.

As increased infiltration of $CD3^+$ T cells together with activated microglia and macrophages in the lumbar spinal cord corresponded to the augmented demyelination in *Cx47* icKO mice compared with *Cx47* fl/fl mice, the exacerbation of acute EAE is likely to be caused by increased infiltration of these immunocytes into the spinal cord, particularly Th17 cells, as shown by flow cytometry of isolated T cells from the CNS tissues. Because MOG-specific Th1 or Th17 cell responses of splenocytes were not altered by the genotypes, the enhanced migration of peripheral immunocytes may be attributable to the proinflammatory milieu in the *Cx47* icKO CNS. Previous articles described that experimental oligodendroglial death did not induce acute neuroinflammation (23, 24). Given the lack of increased inflammatory infiltrates in *Cx32* KO mouse EAE with suspected remyelination failure compared with WT mouse EAE (7), we consider that oligodendroglial death or remyelination failure is not sufficient to induce acute neuroinflammation.

The comparisons of microglia gene expressions by GSEA between *Cx47* icKO and *Cx47* fl/fl mice with TM and EAE, and between TM-injected *Cx47* icKO mice with and without EAE, indicated that augmented induction of proinflammatory and IR phenotype microglia is a characteristic of *Cx47* ablation upon acute autoimmune demyelination. The GO enrichment analysis of isolated microglia using DAVID indicated that the up-regulated DEGs between *Cx47* icKO and *Cx47* fl/fl mice were more enriched in inflammatory response and chemokine-related pathways in the acute EAE phase. Among the genes involved in these dysregulated pathways, isolated microglia from *Cx47* icKO mouse CNS tissues exhibited increased expressions of various chemokines, which can activate Th17 cells (21, 22). Reactivation of myelin-specific T cells through recognition of relevant antigens on antigen-presenting cells in the CNS is indispensable for parenchymal invasion of T cells and emergence of EAE (25). Microglia constitutively expressing MHC class II molecules can serve as nonprofessional antigen-presenting cells in the CNS (25, 26). Moreover, activated microglia can present myelin antigens and activate unprimed and primed myelin antigen-specific T cells (27). Thus, MHC class II-up-regulated microglia in *Cx47* icKO mice are likely to reinforce the CNS-migrated peripheral blood $CD3^+$ T cells by antigen presentation through markedly enriched proinflammatory cytokine gene expressions.

Although the overall antiinflammatory gene expressions in isolated microglia did not differ significantly between *Cx47* icKO and *Cx47* fl/fl mice with TM and EAE, some antiinflammatory transcripts, including *Arg-1*, and $Arg\text{-}1^+$ microglia were more enriched immunohistochemically in *Cx47* icKO mice compared with *Cx47* fl/fl mice. Because Arg-1 is known to possess not only antiinflammatory but also proinflammatory effects (28), the elevation of Arg-1 in *Cx47* icKO mice may exert both beneficial and detrimental effects in our model.

The enrichment of A1-specific and Pan-reactive astroglia-specific gene expressions by GSEA and increase in $C3^+$ astroglia in *Cx47* icKO mice at the acute phase indicate that ablation of oligodendroglial *Cx47* activates astroglia toward proinflammatory characteristics at least in the acute EAE phase. Such proinflammatory astroglia may contribute to proinflammatory activation of microglia and recruitment of peripheral immunocytes to the

CNS via proinflammatory cytokine production. Presumably, strongly activated A1 astrocytes and proinflammatory microglia act in concert to facilitate neuroinflammation at the acute EAE phase in *Cx47* icKO mice.

In the chronic phase, $CD3^+$ T cells infiltrated more abundantly into the spinal cord in *Cx47* icKO mice compared with *Cx47* fl/fl mice, corresponding to the increased relapse numbers and greater clinical severity in *Cx47* icKO mice. Importantly, *Cx47* icKO mice still exhibited activated proinflammatory and IR2 type microglia, according to the GSEA and heat map results, although antiinflammatory microglia were more enriched compared with the preimmunized phase in both *Cx47* icKO and *Cx47* fl/fl mice. GO enrichment analysis of isolated microglia also showed that *Cx47* icKO microglia had more up-regulated gene expressions in inflammatory response and chemokine activity GO terms compared with *Cx47* fl/fl microglia, even at the chronic phase. The expression levels of NOS2 messenger RNA (mRNA) were slightly decreased at the chronic phase of EAE in *Cx47* icKO mice, while the protein levels of NOS2 were increased. However, it is well known that mRNA levels of NOS2 do not always correlate with the protein levels (29, 30). Overall, proinflammatory microglia-related genes were significantly up-regulated in *Cx47* icKO mice compared with *Cx47* fl/fl mice at the chronic phase. By contrast, oligodendroglia-specific gene expressions were more restored in *Cx47* icKO mice than in *Cx47* fl/fl mice. This may partly arise through the emergence of newly differentiated oligodendroglia from oligodendroglia progenitor cells, upon which TM-induced *Cx47* ablation would not work. Collectively, increased demyelination and exacerbation of clinical signs of chronic EAE in *Cx47* icKO mice are not merely caused by oligodendroglia remyelination failure but rather by potentiation of proinflammatory conditions, in clear contrast to chronic EAE in *Cx32* KO mice (7). Although it is possible that *Cx47* ablation may exert peripheral immunomodulatory effects only in the chronic EAE phase, this appears unlikely, because infiltration of $CD3^+$ T cells and macrophages into the CNS tissues decreased over time in the chronic phase of EAE in *Cx47* icKO mice. Therefore, in *Cx47* icKO mice, proinflammatory microglia are likely to recruit $CD3^+$ T cells from the periphery and directly damage neural tissues, leading to increased relapse rates and progressive demyelination.

Cx32/*Cx47* double-KO mice exhibited thin and vacuolated myelin sheaths, demyelinated axons, and axonal loss (14), as well as reduced expressions of oligodendroglia-specific genes (31). Interestingly, these mice also showed activation of microglia and astroglia and infiltration of T and B cells into the CNS parenchyma, which coincided with the increased expressions of microglia-related and lymphocyte-related genes and cytokine/chemokine pathway genes (32, 33). The fact that augmented inflammation in EAE was only seen in *Cx47* icKO mice, and not in *Cx32* KO mice (7), suggests that Cx47 rather than Cx32 plays a pivotal role in regulating CNS inflammation. Because Cx47 forms most heterotypic oligodendroglia–astroglia GJs with Cx43 (10, 32) and astroglial Cx43 expression was unchanged in *Cx47* icKO mice, the remaining Cx43 after loss of oligodendroglia–astroglia GJs could exist as hemichannels. Such Cx43 hemichannels can secrete microglia chemoattractant and toxic molecules, like adenosine 5′-triphosphate and glutamate, and inflammatory chemokines into the extracellular milieu (31, 32). Indeed, Cx43 hemichannel blockade reduced neuroinflammation by suppressing chemokine release (34). Taken together, oligodendroglia-specific *Cx47* ablation disrupts oligodendroglia–astroglia GJs and drives CNS tissues toward a proinflammatory condition, leading to strong attraction of autoimmune T cells and subsequent induction of more severe autoimmune inflammatory demyelination in the CNS at the acute phase.

TM clinically and histologically reduced the severity of acute but not chronic EAE, consistent with its immunosuppressive effects and short degradation time (17). By comparing astroglial and microglial gene expressions between *Cx47* icKO mice with and without TM, we examined the net effects of the immunosuppressive effects of TM and immunopotentiating effects of *Cx47* ablation in the absence of EAE, and found decreased expressions of A1-specific, A2-specific, and Pan-reactive astroglial genes and antiinflammatory and IR-related microglial genes in *Cx47* icKO mice with TM compared with mice without TM at the preimmunized phase. These gene expressions are assumed to be dampened by the stronger immunosuppressive effects of TM over the immunopotentiating effects of *Cx47* ablation at this phase. However, when the effects of TM subsided at the acute phase, increased expressions of Pan-reactive astroglial and IR-related microglial genes became evident in *Cx47* icKO mice with TM, which are likely related to *Cx47* ablation. Furthermore, the comparison of gene expressions by microarray analysis between *Cx47* fl/fl and *Cx47* icKO mice after TM injection but without EAE induction revealed that, in the absence of EAE, *Cx47* ablation by TM injection caused modest changes in astroglial and microglial gene expressions at time points corresponding to the preimmunized and acute phases, except for enhanced Pan-reactive astroglial gene expressions. Thus, it is suggested that the proinflammatory effects of *Cx47* ablation become more apparent upon autoimmune demyelination.

This study has several limitations. First, we focused on in vivo evaluation of the effects of oligodendroglia-specific *Cx47* ablation, but did not perform in vitro functional assays of isolated glial cells. Although the present in vivo assessments have provided a large amount of information on the effects of *Cx47* ablation from mature oligodendroglia, further in vitro functional assays of isolated microglia and other glial cells will complement the present findings. Second, TM-induced *Cx47* ablation using *PLP*/*CreER*^{T} mice does not work on newly formed oligodendroglia from oligodendroglia progenitor cells after the completion of TM injections. Therefore, such newly differentiated oligodendroglia may express Cx47, while oligodendroglial Cx47 is persistently lost in chronic MS plaques (2, 3). Thus, it is plausible that chronic MS lesions may be more prone to neuroinflammation than those in our EAE model, because of sustained loss of Cx47 regulatory control for glial inflammation. Third, we did not to examine the detailed effects of TM on EAE, especially at the chronic phase. Because of the short degradation period of TM (17), the immunosuppressive effects of TM were overwhelmed by the immunopotentiating effects of *Cx47* ablation, even at the acute phase. It is important to note that, despite the immunosuppressive effects of TM as previously reported (15–17), *Cx47* ablation was sufficient to augment acute autoimmune CNS demyelination characterized by enhanced migration of Th17 cells to the CNS and activation of proinflammatory and IR2 microglia and A1 astroglia.

Methods

The experimental procedures were designed to minimize the number of animals used and animal suffering. All animal experiments were performed according to the guidelines for proper conduct of animal experiments published by the Science Council of Japan and the ARRIVE (Animal Research: Reporting of In Vivo Experiments) guidelines for animal research. Ethical approval for the study was granted by the Animal Care and Use Committee of Kyushu University (#A29-146). See *SI Appendix, SI Methods* for detailed information regarding animals, EAE induction by MOG35-55, tissue preparation and immunohistochemistry, quantification of myelin density and cell infiltration, immunoblotting, proliferation assay, multiplexed fluorescent immunoassay, microglia isolation and flow cytometry, gene expression microarray, differential expression analysis, functional analysis of DEGs, and statistical analysis.

Data Availability. The gene array results were uploaded to the Gene Expression Omnibus repository (accession no. GSE121339) on the National Center for Biotechnology Information homepage (https://www.ncbi.nlm.nih.gov/geo/query/acc.cgi?acc=GSE121339). Detailed materials and methods are provided in *SI Appendix, Supplementary Methods* and Tables S1–S9.

ACKNOWLEDGMENTS. This study was supported, in part, by the Practical Research Project for Rare/Intractable Diseases from the Japan Agency for Medical Research and Development (J.-i.K.); Japan Society for the Promotion of Science (JSPS) KAKENHI Grants-in-Aid for Scientific Research (A) (Grant 16H02657) (J.-i.K.), (C) (Grant 16K09694) (R.Y.), and (C) (Grant 26461295) (K.M.) from the Japan Society for the Promotion of Science. The authors gratefully acknowledge financial support from the China Scholarship Council.

1. K. Masaki *et al*., Extensive loss of connexins in Baló's disease: Evidence for an autoantibody-independent astrocytopathy via impaired astrocyte-oligodendrocyte/myelin interaction. *Acta Neuropathol.* **123**, 887–900 (2012).
2. K. Markoullis *et al*., Gap junction pathology in multiple sclerosis lesions and normal-appearing white matter. *Acta Neuropathol.* **123**, 873–886 (2012).
3. K. Masaki *et al*., Connexin 43 astrocytopathy linked to rapidly progressive multiple sclerosis and neuromyelitis optica. *PLoS One* **8**, e72919 (2013).
4. J. C. Hervé, M. Derangeon, Gap-junction-mediated cell-to-cell communication. *Cell Tissue Res.* **352**, 21–31 (2013).
5. S. E. Lutz, C. S. Raine, C. F. Brosnan, Loss of astrocyte connexins 43 and 30 does not significantly alter susceptibility or severity of acute experimental autoimmune encephalomyelitis in mice. *J. Neuroimmunol.* **245**, 8–14 (2012).
6. M. Fang *et al*., Connexin 30 deficiency attenuates chronic but not acute phases of experimental autoimmune encephalomyelitis through induction of neuroprotective microglia. *Front. Immunol.* **9**, 2588 (2018).
7. K. Markoullis *et al*., Disruption of oligodendrocyte gap junctions in experimental autoimmune encephalomyelitis. *Glia* **60**, 1053–1066 (2012).
8. E. Nelles *et al*., Defective propagation of signals generated by sympathetic nerve stimulation in the liver of connexin32-deficient mice. *Proc. Natl. Acad. Sci. U.S.A.* **93**, 9565–9570 (1996).
9. K. A. Kleopa, J. L. Orthmann, A. Enriquez, D. L. Paul, S. S. Scherer, Unique distributions of the gap junction proteins connexin29, connexin32, and connexin47 in oligodendrocytes. *Glia* **47**, 346–357 (2004).
10. N. Kamasawa *et al*., Connexin-47 and connexin-32 in gap junctions of oligodendrocyte somata, myelin sheaths, paranodal loops and Schmidt-Lanterman incisures: Implications for ionic homeostasis and potassium siphoning. *Neuroscience* **136**, 65–86 (2005).
11. E. A. Eugenin *et al*., The role of gap junction channels during physiologic and pathologic conditions of the human central nervous system. *J. Neuroimmune Pharmacol.* **7**, 499–518 (2012).
12. M. Bugiani *et al*., GJA12 mutations in children with recessive hypomyelinating leukoencephalopathy. *Neurology* **67**, 273–279 (2006).
13. B. Odermatt *et al*., Connexin 47 (Cx47)-deficient mice with enhanced green fluorescent protein reporter gene reveal predominant oligodendrocytic expression of Cx47 and display vacuolized myelin in the CNS. *J. Neurosci.* **23**, 4549–4559 (2003).
14. D. M. Menichella, D. A. Goodenough, E. Sirkowski, S. S. Scherer, D. L. Paul, Connexins are critical for normal myelination in the CNS. *J. Neurosci.* **23**, 5963–5973 (2003).
15. B. F. Bebo Jr *et al*., Treatment with selective estrogen receptor modulators regulates myelin specific T-cells and suppresses experimental autoimmune encephalomyelitis. *Glia* **57**, 777–790 (2009).
16. S. Behjati, M. H. Frank, The effects of tamoxifen on immunity. *Curr. Med. Chem.* **16**, 3076–3080 (2009).
17. M. Valny, P. Honsa, D. Kirdajova, Z. Kamenik, M. Anderova, Tamoxifen in the mouse brain: Implications for fate-mapping studies using the tamoxifen-inducible Cre-loxP system. *Front. Cell. Neurosci.* **10**, 243 (2016).
18. S. A. Liddelow *et al*., Neurotoxic reactive astrocytes are induced by activated microglia. *Nature* **541**, 481–487 (2017).
19. A. Kroner *et al*., TNF and increased intracellular iron alter macrophage polarization to a detrimental M1 phenotype in the injured spinal cord. *Neuron* **83**, 1098–1116 (2014).
20. T. R. Hammond *et al*., Single-cell RNA sequencing of microglia throughout the mouse lifespan and in the injured brain reveals complex cell-state changes. *Immunity* **50**, 253–271.e6 (2019).
21. E. E. Kara *et al*., Distinct chemokine receptor axes regulate Th9 cell trafficking to allergic and autoimmune inflammatory sites. *J. Immunol.* **191**, 1110–1117 (2013).
22. H. W. Lim, J. Lee, P. Hillsamer, C. H. Kim, Human Th17 cells share major trafficking receptors with both polarized effector T cells and FOXP3+ regulatory T cells. *J. Immunol.* **180**, 122–129 (2008).
23. G. Locatelli *et al*., Primary oligodendrocyte death does not elicit anti-CNS immunity. *Nat. Neurosci.* **15**, 543–550 (2012).
24. L. J. Oluich *et al*., Targeted ablation of oligodendrocytes induces axonal pathology independent of overt demyelination. *J. Neurosci.* **32**, 8317–8330 (2012).
25. R. M. Ransohoff, B. Engelhardt, The anatomical and cellular basis of immune surveillance in the central nervous system. *Nat. Rev. Immunol.* **12**, 623–635 (2012).
26. E. Ulvestad *et al*., Human microglial cells have phenotypic and functional characteristics in common with both macrophages and dendritic antigen-presenting cells. *J. Leukoc. Biol.* **56**, 732–740 (1994).
27. M. K. Matyszak *et al*., Microglia induce myelin basic protein-specific T cell anergy or T cell activation, according to their state of activation. *Eur. J. Immunol.* **29**, 3063–3076 (1999).
28. W. Zhang *et al*., Arginase activity mediates retinal inflammation in endotoxin-induced uveitis. *Am. J. Pathol.* **175**, 891–902 (2009).
29. J. L. Santos *et al*., Differential sensitivity of C57BL/6 (M-1) and BALB/c (M-2) macrophages to the stimuli of IFN-γ/LPS for the production of NO: Correlation with iNOS mRNA and protein expression. *J. Interferon Cytokine Res.* **26**, 682–688 (2006).
30. S. El-Gayar, H. Thüring-Nahler, J. Pfeilschifter, M. Röllinghoff, C. Bogdan, Translational control of inducible nitric oxide synthase by IL-13 and arginine availability in inflammatory macrophages. *J. Immunol.* **171**, 4561–4568 (2003).
31. Z. C. Ye, M. S. Wyeth, S. Baltan-Tekkok, B. R. Ransom, Functional hemichannels in astrocytes: A novel mechanism of glutamate release. *J. Neurosci.* **23**, 3588–3596 (2003).
32. S. K. Wasseff, S. S. Scherer, Activated immune response in an inherited leukodystrophy disease caused by the loss of oligodendrocyte gap junctions. *Neurobiol. Dis.* **82**, 86–98 (2015).
33. G. Chen *et al*., Connexin-43 induces chemokine release from spinal cord astrocytes to maintain late-phase neuropathic pain in mice. *Brain* **137**, 2193–2209 (2014).
34. M. Cronin, P. N. Anderson, J. E. Cook, C. R. Green, D. L. Becker, Blocking connexin43 expression reduces inflammation and improves functional recovery after spinal cord injury. *Mol. Cell. Neurosci.* **39**, 152–160 (2008).